

# Prediction of forbidden ultraviolet and visible emissions in comet 67P/Churyumov-Gerasimenko

Susarla Raghuram <sup>1</sup>, Anil Bhardwaj<sup>2</sup>, and Marina Galand<sup>1</sup>

<sup>1</sup>Department of Physics, Imperial College London, Prince Consort Road,  
London SW7 2AZ, United Kingdom.

<sup>2</sup>Space Physics Laboratory, Vikram Sarabhai Space Centre, Trivandrum, 695022, India.

Received \_\_\_\_\_; accepted \_\_\_\_\_

---

<sup>1</sup>Corresponding author : raghuramsusarla@gmail.com

## ABSTRACT

Remote observation of spectroscopic emissions is a potential tool for the identification and quantification of various species in comets. CO Cameron band (to trace  $\text{CO}_2$ ) and atomic oxygen emissions (to trace  $\text{H}_2\text{O}$  and/or  $\text{CO}_2$ , CO) have been used to probe neutral composition in the cometary coma. Using a coupled-chemistry emission model, various excitation processes controlling CO Cameron band and different atomic oxygen and atomic carbon emissions have been modelled in comet 67P/Churyumov-Gerasimenko at 1.29 AU (perihelion) and at 3 AU heliocentric distances, which is being explored by ESA's Rosetta mission. The intensities of CO Cameron band, atomic oxygen and atomic carbon emission lines as a function of projected distance are calculated for different CO and  $\text{CO}_2$  volume mixing ratios relative to water. Contributions of different excitation processes controlling these emissions are quantified. We assess how  $\text{CO}_2$  and/or CO volume mixing ratios with respect to  $\text{H}_2\text{O}$  can be derived based on the observed intensities of CO Cameron band, atomic oxygen, and atomic carbon emission lines. The results presented in this work serve as base line calculations to understand the behaviour of low out-gassing cometary coma and compare them with the higher gas production rate cases (e.g. comet Halley). Quantitative analysis of different excitation processes governing the spectroscopic emissions is essential to study the chemistry of inner coma and to derive neutral gas composition.

*Subject headings:* molecular processes — comets : general — comets : 67P/Churyumov-Gerasimenko

## 1. Introduction

Exploration of comets with space missions is critical to probe the coma and to access the detailed features of a cometary nucleus. However, remote spectroscopic observations can provide ample information about the global composition of comets. The coma composition associated with main species can be constrained from the analysis of airglow emissions using ground- and space-based telescopes. This nevertheless requires the quantitative assessment of physical processes that govern these emissions in the coma.

Among many observed cometary ultraviolet and visible airglow spectra, metastable emission lines have gained special interest. Solar resonance fluorescence is not an effective excitation mechanism to populate excited metastable states in the coma due to optically forbidden transitions. The dissociative excitation by photons, suprathermal electrons such as photoelectrons, and thermal recombination of ions are the main channels for producing various species in metastable excited states. By observing the emissions from the daughter products, which are particularly from metastable state, the estimation of mixing ratios of their respective parent species has been done in several comets (Feldman et al. 2004; Bockelée-Morvan et al. 2004). The lifetime of a metastable excited species is shorter ( $\sim 0.7$  s for  $O(^1S)$ ,  $\sim 110$  s for  $O(^1D)$ , and  $\sim 3$  ms for  $CO(a^3\Pi)$ ) compared to their respective parent species (e.g., for  $H_2O$  it is  $\sim 8 \times 10^4$  s $^{-1}$  at 1 AU), and cannot travel large radial distances in the coma from the place of formation without being lost through the emission of photons or quenched in collision. Hence, these forbidden emissions are good tracers to quantify the gas production rates of respective parent species in the coma.

Though water is the dominant species in comets, it is very difficult to access cometary  $H_2O$  infrared emissions from ground-based observatories because of strong absorption by terrestrial water molecules. However, the spatial profiles of cometary  $H_2O$  have been observed by ground-based telescopes by observing non-resonance fluorescence emissions

(Mumma et al. 1995; Mumma et al. 1996; Dello Russo et al. 2000). Since  $\text{H}_2\text{O}$  does not have any transitions in ultraviolet and visible regions, the forbidden emissions of its dissociative metastable products ( $[\text{OI}]$  6300, 6364, 5577, 2972 Å) have been used as tracers. Oxygen atoms that are produced in the  $^1\text{S}$  state, decay 95% of the time to the  $^1\text{D}$  state emitting photons at 5577 Å (green line) wavelength, while 5% of them decay directly to the ground  $^3\text{P}$  state which yields 2972 and 2958 Å emission lines. The radiative decay of  $^1\text{D} \rightarrow ^3\text{P}$  leads to 6300 and 6364 Å emission lines (red-doublet emission). Thus, if the green line is present in a cometary spectrum, the red-doublet must also be present, although the red-doublet can be formed without the green line. The quantification of  $\text{H}_2\text{O}$  in the cometary coma has been done by observing  $[\text{OI}]$  6300 Å emission in many comets (Delsemme & Combi 1976; Delsemme & Combi 1979; Fink & Johnson 1984; Schultz et al. 1992; Morgenthaler et al. 2001). The direct de-excitation of  $\text{O}(^1\text{S})$  yields 2972 Å emission line which has been observed in cometary spectrum only once (Festou & Feldman 1981). Since there are other oxygen bearing species, such as  $\text{CO}_2$  and  $\text{CO}$ , which can also produce these metastable states via dissociative excitation reactions, the observed green to red-doublet emission intensity ratio (hereafter referred as G/R ratio) has been used to confirm the parent source of these emission lines (Cochran 1984, 2008; Cochran & Cochran 2001; Morrison et al. 1997; Zhang et al. 2001; Furusho et al. 2006; Capria et al. 2005, 2008, 2010; Decock et al. 2013; McKay et al. 2012, 2013, 2015). Based on  $\text{O}(^1\text{S})$  and  $\text{O}(^1\text{D})$  photorates calculated by Festou & Feldman (1981), the observed high G/R ratio values ( $> 0.1$ ) were ascribed to large  $\text{CO}_2$  and  $\text{CO}$  volume mixing ratios in the coma (Furusho et al. 2006; Capria et al. 2010; McKay et al. 2012; Decock et al. 2013).

The spin forbidden atomic oxygen emission line  $[\text{OI}]$  1356 Å has also been detected using rocket- and space-borne UV spectrometers in comets (Woods et al. 1986; Sahnou et al. 1993; McPhate et al. 1999). Since fluorescence efficiency (g-factor) for this transition is small to explain the observed intensity, production sources for this emission are attributed

to electron impact excitation mechanisms (Cravens & Green 1978). Bhardwaj et al. (1996) accounted for various electron impact excitation sources to explain the observed emission intensity in comet Halley, which had gas production rate of  $1.3 \times 10^{30} \text{ s}^{-1}$  at 1 AU.

$\text{CO}_2$  is also an important oxygen bearing species in the cometary coma but is difficult to detect directly in the visible and ultraviolet cometary spectra because of the lack of electronic transitions. In order to quantify  $\text{CO}_2$  in comets, CO Cameron band emissions ( $\text{a}^3\Pi \rightarrow \text{A}^1\Pi$ ) have been used as a tracer of  $\text{CO}_2$  by assuming that the excited metastable state  $\text{a}^3\Pi$  (lifetime is  $\sim 3 \text{ ms}$ , Gilijamse et al. 2007) originate primarily from photodissociation of  $\text{CO}_2$  (Weaver et al. 1994, 1997; Feldman et al. 1997). This spin-forbidden electron transition ( $\text{a}^3\Pi \rightarrow \text{A}^1\Pi$ ) yields a band emission in the ultraviolet spectral range 1800–2600 Å. Using Hubble Space Telescope (HST), Weaver et al. (1994) detected this band emission on comet 103P/Hartley 2. The observation of CO Cameron band emission on comet 103P led to the re-examination of International Ultraviolet Explorer (IUE) observed spectra and Feldman et al. (1997) identified this emission on four comets (viz., C/1979 Y1 (Bradfield), 1P/Halley, C/1989 X1 (Austin), C/1990 K1 (Levy)). The volume mixing ratios of CO relative to water have been derived in these comets by assuming that photodissociation of  $\text{CO}_2$  is the main source of  $\text{CO}(\text{a}^3\Pi)$ . However, besides photodissociation of  $\text{CO}_2$ ,  $\text{CO}(\text{a}^3\Pi)$  can also be produced via electron impact and dissociative recombination of CO-bearing species (Weaver et al. 1994; Bhardwaj & Raghuram 2011; Raghuram & Bhardwaj 2012).

Atomic carbon [CI] 1931 Å emission line has been observed in several comets (Feldman & Brune 1976; Smith et al. 1980; Feldman et al. 1980; Feldman et al. 1997; Tozzi et al. 1998). The excited state of this emission is a metastable state  $\text{C}(\text{}^1\text{D})$  which has a lifetime of about 4080 s (Hibbert et al. 1993). The radiative decay of carbon from  $\text{}^1\text{D}$  to the ground  $\text{}^3\text{P}$  state results in photons at 9823 and 9850 Å, which are analogous to atomic oxygen red-doublet emissions at 6300 and 6464 Å. The [CI] 9850 Å emission line has been detected

in comet Hale-Bopp by Oliverson et al. (2002). The carbon atom in  $^1\text{D}$  metastable state fluoresces the solar photons at  $1931 \text{ \AA}$  before radiative decay to the ground  $^3\text{P}$  state can occur. Most of the emission line intensity is attributed to photodissociative excitation of CO in comets (Feldman 1978; Bhardwaj 1999). Hence this emission line is a good tracer for CO production rate in comets (Oliverson et al. 2002). The model developed by Bhardwaj (1999) calculated this emission line intensity in comet Halley, which is smaller by a factor 5 than that observed by IUE, and suggested an involvement of additional carbon-bearing species in the coma.

In order to derive the parent species production rates in the coma based on the observed forbidden emission intensities a quantitative study of various processes that govern these emissions is necessary. We have developed a coupled chemistry-emission model which accounts for major production and loss reactions of  $\text{O}(^3\text{P})$ ,  $\text{O}(^1\text{S})$ ,  $\text{O}(^1\text{D})$ ,  $\text{C}(^3\text{P})$ ,  $\text{C}(^1\text{D})$ , and  $\text{CO}(a^3\Pi)$  in cometary comae (Bhardwaj et al. 1996; Bhardwaj 1999; Bhardwaj & Raghuram 2011, 2012). This model has been applied on several comets and results have been compared with the Earth-based observations (Bhardwaj et al. 1996; Bhardwaj 1999; Bhardwaj & Raghuram 2011, 2012; Raghuram & Bhardwaj 2012, 2013, 2014; Decock et al. 2015). The model calculations for comets 103P/Hartley 2 and 1P/Halley have shown that suprathermal electron impact is an important excitation process in the formation of  $\text{CO}(a^3\Pi)$ , which is more important than photodissociation of  $\text{CO}_2$  (Bhardwaj & Raghuram 2011; Raghuram & Bhardwaj 2012). The model applied to study atomic oxygen emission lines in comets has shown that the collisional quenching in the inner coma can significantly change the observed G/R ratio (Bhardwaj & Raghuram 2012; Raghuram & Bhardwaj 2013, 2014; Decock et al. 2015). The model calculations in active comets, such as (C/1996 B2) Hyakutake and (C/1995 O1) Hale-Bopp, have shown that the G/R ratio varies as a function of projected distance and depends on the collisions in the cometary comae (Bhardwaj & Raghuram 2012; Raghuram & Bhardwaj 2013). Recently, we have applied our model for the analysis

of high-resolution spectroscopic observations made from ESO very large telescope (VLT) on four comets (viz., C/2002 T7 (LINEAR), 73P-C/Schwassmann-Wachmann 3, 8P/Tuttle, and 103P/Hartley 2). This study has allowed to constrain the CO<sub>2</sub> volume mixing ratios in these comets (Decock et al. 2015).

After a successful rendez-vous in August 2014, ESA’s Rosetta spacecraft is exploring comet 67P/Churyumov-Gerasimenko (here-after, referred as 67P) by escorting it from  $\sim 4$  AU towards perihelion at 1.29 AU reached in the summer 2015. Assessing the chemical evolution of the cometary coma, as the comet approaches the Sun, is one of the main aims of Rosetta mission. In support to Rosetta, different space- and ground-based observation campaigns are taking place to understand the spatial distribution of different volatile species in the coma. We apply our coupled chemistry-emission model to comet 67P to identify and quantify the processes driving formation and loss of CO Cameron band, atomic oxygen forbidden emissions and [CI] 1931 Å emission line at perihelion and at 3 AU heliocentric distance. Model calculations are necessary to understand the physical processes governing these metastable emissions and to derive CO<sub>2</sub> and CO mixing ratios. The motivation for this work is to provide a theoretical support for the interpretation of Earth-based and Rosetta-based UV observations of comet 67P.

We present the model input parameters, which may represent the gaseous environment of comet 67P at its perihelion and at 3 AU, in section 2. The modelled various production and destruction profiles for different electronic states of atomic oxygen, and atomic carbon, and CO(a<sup>3</sup>Π), and emission intensities as a function of projected distance are presented in section 3. The implications of modelled emission profiles for comet 67P are discussed in section 4. Conclusions are given in section 5.

## 2. Model input parameters

The coupled chemistry-emission model has been used in the present study which accounts for main production and loss processes for  $\text{CO}(\text{a}^3\Pi)$ ,  $\text{O}(\text{}^3\text{P})$ ,  $\text{O}(\text{}^1\text{D})$ ,  $\text{O}(\text{}^1\text{S})$ ,  $\text{C}(\text{}^3\text{P})$ , and  $\text{C}(\text{}^1\text{D})$  species in the inner cometary coma, as described in the earlier works (Bhardwaj & Raghuram 2011, 2012; Bhardwaj et al. 1990, 1996; Bhardwaj 1999, 2003). Calculations are done at perihelion distance (1.29 AU). The  $\text{H}_2\text{O}$  out-gassing rate at perihelion is assumed to be  $1 \times 10^{28} \text{ s}^{-1}$  (Snodgrass et al. 2013). The number density relative to water is taken to be 5% for both  $\text{CO}_2$  (hereafter  $\mu_w(\text{CO}_2)$ ) and  $\text{CO}$  (hereafter  $\mu_w(\text{CO})$ ) as a standard neutral composition. The on-board OSIRIS instrument on Rosetta mission observed 67P’s nucleus has bi-lobed structure with dimension  $2.5 \times 2.5 \times 2.0 \text{ km}$  for the small lobe and  $4.1 \times 3.2 \times 1.3 \text{ km}$  for the large lobe (Sierks et al. 2015; Lee et al. 2015). In our model we have assumed a spherical nucleus of 2 km radius for simplification. The neutral atmosphere is calculated using Haser’s formula (Haser 1957) which assumes spherical expansion of coma with a constant velocity of  $1 \text{ km s}^{-1}$ . The electron temperature profile, which is required to calculate electron-ion recombination rate, is assumed to be same as on Halley (Körösmezey et al. 1987).

We vary  $\text{CO}_2$  and  $\text{CO}$  mixing ratios to quantify the change in contributions of different productions and loss processes yielding  $\text{CO}(\text{a}^3\Pi)$ ,  $\text{O}(\text{}^1\text{S})$ ,  $\text{O}(\text{}^1\text{D})$ ,  $\text{C}(\text{}^1\text{D})$ , and atomic carbon and atomic oxygen in ground states. The incident solar flux is based on the measurements from the Thermosphere Ionosphere Mesosphere Energetics and Dynamics (TIMED)/Solar EUV Experiment (SEE) (Woods et al. 2005) on 2 January 2005 (for solar activity phase with  $\text{F10.7} = 100 \times 10^{22} \text{ Wm}^{-2} \text{ Hz}^{-1}$ ) at Earth and scaled to heliocentric distance of 1.29 AU. It is expected to be representative of conditions encountered in summer 2015 near perihelion from solar decreasing active period (Vigren & Galand 2013). The theoretical water collisional zone of comet 67P, with gas production rate  $10^{28} \text{ s}^{-1}$ , is around 2000 km



(Whipple & Huebner 1976). The calculations presented in this work are relevant for the inner coma and inside the diamagnetic cavity.

We also made calculations at heliocentric distance of 3 AU assuming the total gas production rate of  $5 \times 10^{25} \text{ s}^{-1}$  (Gulkis et al. 2015; Hässig et al. 2015; Bieler et al. 2015). The neutral coma composition is assumed to be 80%  $\text{H}_2\text{O}$ , 15%  $\text{CO}$  and 5%  $\text{CO}_2$ . The solar flux on 1 November 2014 is used in the model and scaled to 3 AU using inverse square of heliocentric distance. The electron temperature-dependent reactions play a minor role in governing the intensities of these emission lines.

Recently ROSINA/DFMS has made several important discoveries such as the D/H ratio (Altwegg et al. 2015), presence of  $\text{N}_2$  (Rubin et al. 2015) and  $\text{O}_2$  (Bieler et al. 2015) in 67P’s coma. The observation of molecular oxygen has an important implication in the production of  $\text{O}(^1\text{S})$  and  $\text{O}(^1\text{D})$ . Bieler et al. (2015) found that the local abundance of molecular oxygen is varying between 1 and 10% around the 67P nucleus relative to  $\text{H}_2\text{O}$  production rate. The mean value of molecular oxygen abundance in 67P coma is  $3.8 \pm 0.85\%$  relative to  $\text{H}_2\text{O}$  production rate (Bieler et al. 2015). In order to quantify the contribution of molecular oxygen on the forbidden emission lines we have taken 4% molecular oxygen relative to  $\text{H}_2\text{O}$  production rate in the model. Hence we also have done a case study by assuming the water production rate  $5 \times 10^{25} \text{ s}^{-1}$  and 25%  $\text{CO}$ , 8.3%  $\text{CO}_2$ , and 4%  $\text{O}_2$  as relative abundances with respect to  $\text{H}_2\text{O}$  for the month of August 2014. These abundances are mostly in agreement with the ROSINA measurements between August and October 2014 (Hässig et al. 2015; Le Roy et al. 2015; Bieler et al. 2015) when the comet was between 3 and 3.5 AU from the Sun.

### 3. Results

#### 3.1. Formation and destruction of $\text{CO}(\text{a}^3\Pi)$

The modelled  $\text{CO}(\text{a}^3\Pi)$  rate profiles for different formation processes in the coma of 67P are shown in Figure 1. The number of excited  $\text{CO}(\text{a}^3\Pi)$  molecules produced per unit volume per second is referred to as volumetric production rate. For equal (5% relative to water)  $\text{CO}_2$  and CO volume mixing ratios relative to water in the coma the major production sources of  $\text{CO}(\text{a}^3\Pi)$  is electron impact on CO. The electron impact on  $\text{CO}_2$  and photodissociation of  $\text{CO}_2$  are next most dominant sources of  $\text{CO}(\text{a}^3\Pi)$ . The thermal electron recombination of  $\text{HCO}^+$  and  $\text{CO}_2^+$  ions and fluorescence of CO are minor  $\text{CO}(\text{a}^3\Pi)$  production sources. Above 500 km the contributions from photodissociative excitation of  $\text{CO}_2$  and electron impact on CO and  $\text{CO}_2$  are nearly equal. Since the lifetime of  $\text{CO}(\text{a}^3\Pi)$  is short ( $\sim 3$  ms, Gilijamse et al. 2007), most of the excited molecules decay to ground state by spontaneous emission. Hence the radiative decay is the major loss source of this excited state. Other loss processes, such as collisional quenching and ionization by photons and photoelectrons, are smaller compared to radiative decay by several orders of magnitude. The number of species de-excite to ground state per second by various loss mechanisms is referred to as loss rate.

The cross section for electron impact excitation of various excited states and the calculated suprathermal electrons intensity in 67P coma at 10 km radial distance is presented in Figure 2. The suprathermal electrons intensity in the energy range between 10–15 eV mainly determines the excitation rate of  $\text{CO}(\text{a}^3\Pi)$  through electron impact on CO bearing species.

### 3.2. Formation and destruction of atomic oxygen and atomic carbon

#### 3.2.1. Atomic oxygen in $^3P$ , $^1D$ , $^1S$ , and $^5S$ states

The modelled major production rate profiles of atomic oxygen and atomic carbon in ground states are presented in Figure 3. Below 50 km radial distances, various sources are contributing to the formation of  $O(^3P)$ . The production of atomic oxygen in ground state is mainly due to strong collisional quenching of  $O(^1D)$  with water. The next important sources of atomic oxygen are charge exchange of  $OH^+$  and  $O^+$  ions with water. Photodissociation of  $CO_2$  and  $CO$  are next important  $O(^3P)$  production sources. Above 50 km radiative decay of  $O(^1D)$  is the major source of atomic oxygen in ground state.

The calculated major chemical loss rate profile for  $O(^3P)$  via different destruction mechanisms are presented in Figure 4. The major loss process for the atomic oxygen is due to collisions with  $OH$  molecules which yields atomic hydrogen and molecular oxygen. The atomic oxygen can travel to large distances before getting lost in chemical reactions. Hence, we accounted transport loss by taking  $1 \text{ km s}^{-1}$  as advection velocity.

We have accounted for many  $O(^1S)$  and  $O(^1D)$  formation and destruction processes in the coma as described in Bhardwaj & Raghuram (2012). The modelled major production rate profiles for  $O(^1S)$  in comet 67P are shown in Figure 5. The photodissociation of  $H_2O$  and  $CO_2$  are equally important sources in producing  $O(^1S)$  in the inner coma of comet 67P. Below 100 km, suprathermal electron impact on  $CO_2$  is next important  $O(^1S)$  source. The photodissociation of  $CO$  and electron impact on  $H_2O$  and  $CO_2$  are minor sources of  $O(^1S)$ . Electron recombination of  $H_2O^+$  ion is a minor source of  $O(^1S)$  in the inner coma whereas its contribution is significant at large ( $>10^3 \text{ km}$ ) radial distances.

The calculated  $O(^1D)$  production rates profiles for different formation processes are presented in Figure 6. The photodissociation of  $H_2O$  is a dominant source of  $O(^1D)$

throughout the inner coma. Contribution from other  $O(^1D)$  formation processes is minor ( $<5\%$  to the total). At large radial distances ( $> 10^3$  km) the contributions from dissociative recombination of  $H_2O^+$ , radiative decay of  $O(^1S)$  and photodissociation of OH become significant in the formation of  $O(^1D)$ .

The modelled destruction rate profiles of  $O(^1S)$  and  $O(^1D)$  are shown in Figure 7. The  $O(^1S)$  and  $O(^1D)$  atoms are strongly quenched by  $H_2O$  up to radial distances of  $\sim 10$  and  $\sim 200$  km, respectively. Above these radial distances the radiative decay, which leads to forbidden visible emission lines, is the major loss process for the  $O(^1S)$  and  $O(^1D)$ . Collisional quenching of  $O(^1S)$  and  $O(^1D)$  by other neutrals is smaller compared to  $H_2O$  quenching by several orders of magnitude, hence these processes are not shown in the figure.

The production of atomic oxygen in  $^5S$  state yields [OI] 1356 Å emission line via immediate decay to ground state (lifetime is 185  $\mu s$ , Johnson 1972). The calculated [OI] 1356 Å emission rates are presented in Figure 8. Electron impact on atomic oxygen is the major production source for [OI] 1356 Å emission followed by electron impact on  $CO_2$  and  $H_2O$ .

### 3.2.2. Atomic carbon in $^3P$ and $^1D$ states

In case of atomic carbon formation the photodissociation of CO is the major source of  $C(^3P)$  as shown in Figure 3. Collisional quenching of  $C(^1D)$  is next important source of atomic carbon in ground state. All other production processes described in Bhardwaj et al. (1996) contribute little ( $<5\%$ ) to the total. The loss of atomic carbon is mainly due to collisions with OH which yields atomic hydrogen and CO. The next main loss source is due to collisions with  $H_3O^+$  which leads to the formation of  $HCO^+$  and  $H_2$ . The model accounts for transport of atomic carbon in  $^3P$  and  $^1D$  states with an advection velocity of 1 km  $s^{-1}$ .

Transport is the major loss processes for atomic oxygen and atomic carbon compared to the total loss due to chemical reactions.

The calculated formation rates of metastable  $C(^1D)$  atom via different production processes are presented in Figure 9. The major formation mechanism for  $C(^1D)$  is photodissociation of CO. At large radial distance ( $10^3$  km) dissociative recombination of  $CO^+$  ion is also an important source of  $C(^1D)$ . Other formation reactions are smaller compared to photodissociation of CO by more than an order of magnitude. The modelled  $C(^1D)$  loss rates presented in Figure 10 show that the collisional quenching with water is the dominant loss process up to 300 km radial distance, above which radiative decay takes over. Collisional quenching of CO and  $CO_2$  are relatively less significant  $C(^1D)$  loss processes.

### 3.3. Calculation of emission intensities along the projected distance

The radial emission rate profiles are integrated for each emission line along the line-of-sight perpendicular to the Sun-comet direction at different radial distances to obtain limb brightness profiles. The model calculated intensity profiles, as a function of projected distance, for CO Cameron band, atomic oxygen ( [OI] 6300+6364 Å, 5577 Å, 2972 Å, and 1356 Å) and atomic carbon emissions ([CI] 1931, 9823, 9850 Å) are shown in Figure 11. Among the calculated emission intensities CO Cameron band emission peaks close to the nucleus (<20 km). The calculated intensity profiles of 5577 Å and red-doublet (6300+6364 Å) are flat up to radial distances 20 km and 200 km, respectively, due to strong collisional quenching of  $O(^1S)$  and  $O(^1D)$  with  $H_2O$  in the inner coma. The calculated G/R ratio as a function of projected distance is also presented in the same figure on the right Y-axis. Since lifetime of metastable  $C(^1D)$  is large (4080 s), the collisional quenching with water makes [CI] 1931, 9850 and 9823 Å emission profiles flat up to 1000 km. The [OI] 1356 Å line is the weakest emission among the calculated emissions (presented in Figure 11

after multiplying a factor 10).

Model calculated intensity profiles, when comet was at 3 AU heliocentric distance, are presented in Figure 12 as a function of projected distance. Very close to the nucleus surface the oxygen red-doublet, green line, CO Cameron, and [OI] 1356 Å emissions are intense. Since neutral gas production rate is low ( $5 \times 10^{25} \text{ s}^{-1}$ ) at 3 AU the calculated intensity profiles are decreased by two order of magnitude compared to those at perihelion. Due to high radiative lifetime ( $\sim 110 \text{ s}$ ), the collisional quenching of  $\text{O}(^1\text{D})$  is significant for radial distance up to 20 km, which alters the G/R ratio from 0.9 to 0.1. In spite of having high mixing ratio (15%), the role of CO in determining the oxygen visible emission intensities as well as in determining the G/R ratio is insignificant. In the case of CO Cameron band, most of emission intensity ( $>90\%$ ) close to nucleus is mainly via electron impact excitation of CO. For radial distance higher than 50 km, the major ( $\sim 50\%$ ) source for  $\text{CO}(\text{a}^3\Pi)$  is  $\text{CO}_2$  via electron impact and photodissociation excitation processes. The long radiative lifetime ( $\sim 4080 \text{ s}$ ) of  $\text{C}(^1\text{D})$  makes the atomic carbon emission intensity profile flat up to 1000 km.

### 3.4. Effect of neutral composition on the calculation of emission intensities

#### 3.4.1. Role of $\text{CO}_2$ and CO volume mixing ratios relative to water

By varying the  $\mu_w(\text{CO}_2)$  and  $\mu_w(\text{CO})$  the contribution of different processes producing  $\text{CO}(\text{a}^3\Pi)$  is calculated at three different projected distances. The calculations are presented in Table 1 by varying  $\mu_w(\text{CO}_2)$  and  $\mu_w(\text{CO})$  from zero to two, and then to five percent. In all these cases the contribution from photodissociation of  $\text{CO}_2$  and electron impact on  $\text{CO}_2$  processes are nearly equal. Keeping 1%  $\mu_w(\text{CO}_2)$  in the coma we varied  $\mu_w(\text{CO})$  between 1 and 5%. In this case the contribution of photodissociation of  $\text{CO}_2$  and electron impact on  $\text{CO}_2$  in the inner coma is  $<15\%$ , whereas electron impact on CO is about 65–90%. The

contribution from other chemical reactions, such as electron recombination of  $\text{HCO}^+$  and  $\text{CO}_2^+$  ions contribute less than 10% to the formation of  $\text{CO}(\text{a}^3\Pi)$ .

When  $\mu_w(\text{CO}_2)$  is increased to 2%, the contribution from electron impact on CO is reduced to 50–80%. About 10–20% of  $\text{CO}(\text{a}^3\Pi)$  is produced from photodissociation of  $\text{CO}_2$ . By increasing  $\mu_w(\text{CO}_2)$  to 5% the contribution of  $\text{CO}_2$ , from both photodissociation and electron impact reactions, in producing  $\text{CO}(\text{a}^3\Pi)$  increases to a total of 30 – 60%. In the case of equal (5%)  $\mu_w(\text{CO})$  and  $\mu_w(\text{CO}_2)$ , the contribution from CO is around 65% and the rest comes from  $\text{CO}_2$ -associated reactions in the inner coma.

Modelling results in Table 1 show that in the absence of  $\text{CO}_2$  the main source for production of  $\text{CO}(\text{a}^3\Pi)$  is electron impact of CO and other processes have negligible contribution to the total. When CO is absent in the coma electron impact on  $\text{CO}_2$  and photodissociation of  $\text{CO}_2$  processes are producing  $\text{CO}(\text{a}^3\Pi)$  with nearly equal contributions. In this case at 1000 km projected distances, the contribution of the thermal recombination of  $\text{HCO}^+$  and  $\text{CO}_2^+$  producing  $\text{CO}(\text{a}^3\Pi)$  is 15%.

The calculated percentage contribution of different processes in the formation of  $\text{O}(\text{1S})$  and  $\text{O}(\text{1D})$  are presented in Table 2. The main processes controlling the formation of  $\text{O}(\text{1S})$  is photodissociation of  $\text{H}_2\text{O}$  and  $\text{CO}_2$ . The photodissociation of  $\text{H}_2\text{O}$  is the dominant source of  $\text{O}(\text{1D})$  production in the inner coma. Beyond 1000 km radial distances, the photodissociation of OH, electron recombination of  $\text{H}_2\text{O}^+$ , and radiative decay of  $\text{O}(\text{1S})$  are also important  $\text{O}(\text{1D})$  sources. The calculations presented in Table 2 show that below 100 km radial distance the formation of  $\text{O}(\text{1D})$  is mainly (80–90%) through photodissociation of  $\text{H}_2\text{O}$ . Above these distances this contribution changes to around 50%, while the rest is via photodissociation of OH and dissociative recombination of  $\text{H}_2\text{O}^+$  and radiative decay of  $\text{O}(\text{1S})$ .

In the case of  $\text{O}(\text{1S})$  production, both photodissociation of  $\text{CO}_2$  and  $\text{H}_2\text{O}$  are important

formation processes in the inner coma. It is found that the role of CO photodissociation is very small ( $<5\%$ ) in the  $O(^1S)$  production. Calculations presented in Table 2 show that for 1% of  $\mu_w(\text{CO}_2)$ , below 100 km projected distance, the contributions in the formation of  $O(^1S)$  are 65–75% from photodissociation of  $\text{H}_2\text{O}$ , 15% from  $\text{CO}_2$  photodissociation, and 20% from other reactions. At 1000 km projected distance the photodissociation of  $\text{H}_2\text{O}$  is contributing around 45% and  $\sim 45\%$  contribution mainly from dissociative recombination of  $\text{H}_2\text{O}^+$ . In this case the calculated G/R ratio varies between 0.05 and 0.4 for less than 1000 km projected distance. When we increased  $\mu_w(\text{CO}_2)$  to 5% the contribution from both photodissociation of  $\text{H}_2\text{O}$  and  $\text{CO}_2$  is similar (30 to 45%) for the projected distances less than 1000 km. In this case G/R ratio is found to vary between 0.07 to 0.7.

In the absence of  $\text{CO}_2$ , the photodissociation of water and dissociative recombination of  $\text{H}_2\text{O}^+$  mainly controls the formation of  $O(^1S)$  in the cometary coma. In this case by changing the CO alone between 1 and 5%, it is found that the change in the calculated G/R ratio profile is insignificant. Assuming the absence of CO in the coma, the calculated contributions are not changed from the previous cases whereas the calculated G/R ratio profile is increasing linearly by increasing  $\mu_w(\text{CO}_2)$ .

We have calculated the  $[\text{OI}]$  1356 Å emission intensity by varying  $\mu_w(\text{CO}_2)$  and  $\mu_w(\text{CO})$  between 1% and 5%. The calculations show that electron impact on atomic oxygen is important (50%) excitation process for  $[\text{OI}]$  1356 Å emission (see Figure 8). Electron impact on  $\text{CO}_2$  is next important emission source of  $[\text{OI}]$  1356 Å line (30% to the total). Below 50 km, the formation of atomic oxygen is through collisional quenching of  $O(^1D)$  with water (35%), charge exchange between  $\text{O}^+$  and  $\text{OH}^+$  with water (45%). Above this radial distance 75% atomic oxygen is produced due to radiative decay of  $O(^1D)$ . The role of  $\text{CO}_2$  and CO in producing atomic oxygen is less than 5%. Hence, by increasing the  $\mu_w(\text{CO}_2)$  in the coma it is found that 30% of this emission line intensity is increased only below 50 km



radial distance. The role of CO in producing this emission line is insignificant.

The  $\mu_w(\text{CO})$  can significantly influence the [CI] 1931 Å emission intensity compared to that of CO<sub>2</sub>. By increasing the  $\mu_w(\text{CO})$  from 1 to 5% it is found that the intensity of this emission line also increases. The [CI] 1931 Å is mainly through photodissociation of CO (75%) and CO<sub>2</sub> (20%). The role of resonant scattering of C(<sup>1</sup>D) is significant (50%) for radial distances larger than 500 km. Similar effects also have been observed on 9850 and 9823 Å emission lines.

### 3.4.2. Role of H<sub>2</sub>O gas production rate

The maximum gas production in this comet at perihelion for high activity case is about  $1 \times 10^{28} \text{ s}^{-1}$ . We have also done calculations for this comet by considering low activity case with water production rate of  $5 \times 10^{27} \text{ s}^{-1}$  and keeping the  $\mu_w(\text{CO}_2)$  and  $\mu_w(\text{CO})$  equal (5%). By decreasing the gas production rate by a factor of 2 it is found that the calculated emission intensities are decreased by 30%. Similarly the collisional quenching radius for O(<sup>1</sup>S), O(<sup>1</sup>D), and C(<sup>1</sup>D) also decreased by 30% and is moved towards the nucleus.

## 4. Discussion

### 4.1. Spectroscopic observations at comet 67P

ALICE ultraviolet spectrometer on-board Rosetta mission is designed to observe many emission lines from 67P in the wavelength region 750 – 2050 Å (Stern et al. 2007; Feldman et al. 2011). This range overlaps with part of CO Cameron bands covering 1800–2600 Å, [OI] 1356 Å, and [CI] 1931 Å emission lines (Stern et al. 2007; Feldman et al. 2004). By making limb scan observations ALICE spectrograph can be used to derive the spatial

distribution of CO and/or CO<sub>2</sub> around 67P nucleus. ALICE can observe the shortward part of CO Cameron band emission in its longward limit where unfortunately the sensitivity is small (Stern et al. 2007). Similarly [CI] 1931 Å emission line also falls into the longer end of the ALICE spectral range. It may however possible to detect it because of strong resonant fluorescence efficiency of C(<sup>1</sup>D) atom. The Rosetta onboard Optical, Spectroscopic, and Infrared Remote Imaging System (OSIRIS) is a scientific camera system with 12 discrete filters which is designed to observe 67P cometary coma over the wavelength range 250–1000 nm (Keller et al. 2007). OSIRIS can also map the release of certain daughter species such as OH and [OI] based on observed emission intensities at 3090 Å and at 6300 Å, respectively.

Outcome of this study can be compared with on-board ROSINA mass spectrometers in-situ measurements of the neutral composition in the coma (Balsiger et al. 2007; Hässig et al. 2015). Space-based observations from Earth, such as from the Hubble Space Telescope (HST), can also observe these ultraviolet emissions during Rosetta mission observation period. Several ground-based observatories have been observing comet 67P (<http://www.rosetta-campaign.net/planned-observations>) in visible and infrared regions to study the spatial distribution of various species. In this context the present modelling work can provide better understanding of different processes governing CO Cameron band, atomic oxygen and atomic carbon emission lines in comet 67P to derive parent neutral composition in the coma.

#### **4.2. Derivation of CO and CO<sub>2</sub> volume mixing ratios relative to H<sub>2</sub>O close to the nucleus**

By making several observations on different comets Tozzi et al. (1998) demonstrated that there is a strong correlation between 1931 Å emission line intensity and CO column density. The radiative decay of C(<sup>1</sup>D) to ground state yields 9823 and 9850 Å emission

lines. By observing these emission lines on Hale-Bopp, Oliverson et al. (2002) concluded that they can be used as direct tracers of CO photodissociation in the cometary coma. The model calculations also show that the major production source of C(<sup>1</sup>D) in the inner coma is mainly due to photodissociation of CO and the contribution from other production processes is smaller by an order of magnitude compared to the former (see Fig 9). The model calculated 1931, 9850, and 9823 Å emission line profiles are flat up to 1000 km projected distances due to strong collisional quenching of C(<sup>1</sup>D) with H<sub>2</sub>O. Since these atomic carbon emission lines are mainly controlled by photodissociation of CO, observed intensity profiles can be used to derive the CO gas production rate in the coma. The calculated emission intensity profile can be useful as a baseline prediction to constrain the CO mixing ratios in the coma for the Alice observation of carbon emission lines which can be then compared with the ROSINA observations for the same regions under similar solar illumination.

Measuring atomic oxygen visible emission line intensities is an important diagnostic tool in estimating the water production rate as well as to understand the spatial distribution of H<sub>2</sub>O in the cometary coma (Delsemme & Combi 1976; Delsemme & Combi 1979; Fink & Johnson 1984; Schultz et al. 1992; Morgenthaler et al. 2001; Furusho et al. 2006). Decock et al. (2015) analysed several ESO’s VLT observed high resolution green and red-doublet emission line spectra on various comets. CO<sub>2</sub> mixing ratios are derived in these comets by comparing the ESO VLT observations with modelled G/R ratio profiles (Decock et al. 2015). The model calculated G/R ratio profile is presented on 67P in Figure 11. By modelling green and red-double emission intensity profiles on various comets at different heliocentric distances, Raghuram & Bhardwaj (2014) have shown that G/R ratio value increases linearly by increasing  $\mu_w(\text{CO}_2)$  in the coma whereas the affect of CO is minor in determining either green or red-doublet emission intensities. Hence, the observed G/R ratio profile on 67P can be used to constrain CO<sub>2</sub> mixing ratio in the coma.

When a comet is far away from the Sun (3 AU), it is expected to have higher CO and CO<sub>2</sub> volume mixing ratios which are species associated with low sublimation temperatures (e.g., Mumma & Charnley 2011). The calculations made at 3 AU heliocentric distance (see Fig. 12), with mixing ratios 5% CO<sub>2</sub> and 15% CO, show that atomic oxygen red-doublet emission is the most intense emission in the inner coma. This emission can be observed by Rosetta onboard OSIRIS instrument which can be subsequently used to derive water production rate. Unfortunately there are no filters on OSIRIS to measure [OI] 5577 Å, [CI] 9823 Å, and 9850 Å emission lines (Keller et al. 2007). The predicted oxygen red-doublet intensity along the projected distance (Figures 11 and 12) could be useful in analysing OSIRIS visible spectra of 67P and subsequently deriving H<sub>2</sub>O distribution around the nucleus.

#### 4.3. Constraining the O(<sup>1</sup>S) yield for H<sub>2</sub>O at solar Ly-α wavelength

The photon cross section for the formation of O(<sup>1</sup>S) from H<sub>2</sub>O has never been reported in the literature (Huestis & Slanger 2006). In this model the formation of O(<sup>1</sup>S) from photodissociation of H<sub>2</sub>O has been accounted by assuming 0.5% yield for H<sub>2</sub>O at Ly-α wavelength (Bhardwaj & Raghuram 2012). The onboard ROSINA spectrometers can measure the CO<sub>2</sub> number densities during this mission period at different radial distances in the coma. By combining the observed G/R ratio profile with onboard ROSINA CO<sub>2</sub> measurements it would be possible to constraint the O(<sup>1</sup>S) average yield value at solar Lyman-α. The high-resolution spectroscopic observations, such as analysis of Decock et al. (2015), can provide information about collisional quenching of O(<sup>1</sup>S) and O(<sup>1</sup>D) metastable states in the coma of 67P. The observation of both green and red-doublet emission line widths and G/R ratio profiles along with ROSINA measurements can solve the puzzle that green line is wider than either of red-doublet emission lines in comets.

#### 4.4. Derivation of suprathermal electron intensity close to the nucleus

The modelling of production rates of  $\text{CO}(\text{a}^3\Pi)$  has shown that suprathermal electron impact reactions mainly govern the CO Cameron band emission with contribution of around 75% whereas  $\text{CO}_2$  photodissociation contributes about 25% (see section 3.1). In the absence of CO, the electron impact on  $\text{CO}_2$  is an equally important production source of  $\text{CO}(\text{a}^3\Pi)$  as photodissociation of  $\text{CO}_2$  (see Table 1). This suggest that electron impact excitation mechanism should be considered for the estimation of parent species production rates in the coma. With sufficient CO ( $\geq 3\%$ ) in the coma, the contribution from electron impact reactions in producing this band emission close to the nucleus ( $< 100$  km) is about 80%. The excited state  $\text{CO}(\text{a}^3\Pi)$  is mainly populated in the coma by suprathermal electrons in the energy range between 10 and 15 eV (see Figure 2). Since the major source for the production of  $\text{CO}(\text{a}^3\Pi)$  is electron impact, the observed CO Cameron band emission close to the nucleus would be suitable to track the suprathermal electron intensity (McPhate et al. 1999) rather than  $\text{CO}_2$  neutral density.

The  $[\text{OI}]$  1356 Å emission line is an excellent tracer for electron impact processes in the coma. Modelling of electron impact excitation processes shows that this emission is mainly due to electron impact excitation of atomic oxygen followed by electron impact dissociative emission of  $\text{CO}_2$  and  $\text{H}_2\text{O}$  (see Figure 8). However, the intensity of this emission is weaker by three orders of magnitude compared to CO Cameron band emission. The electron impact excitation cross section for atomic oxygen producing  $[\text{OI}]$  1356 Å emission line peaks at 15 eV whereas for  $\text{CO}_2$  and  $\text{H}_2\text{O}$  it is between 30 and 60 eV. The contribution from atomic oxygen is about 50% and the rest is through  $\text{CO}_2$  (30%) and  $\text{H}_2\text{O}$  (20%). Hence, half of the observed emission intensity profile is linked to the suprathermal electron intensity at 15 eV. Recently ALICE observed several HI, OI, and CI emission near the cometary nucleus when comet was at around 3 AU (Feldman et al. 2015). The observation of OI 1356 Å emission

line intensity, which is varying between  $\sim 1.5$  and  $\sim 3$  Rayleigh at 10 km projected distance, (Feldman et al. 2015), is close to our predicted calculation ( $\sim 1.5$  Rayleigh, see Fig. 12). Detailed analysis of this emission line will be presented in the future work using the Rosetta measured neutral density distribution around the nucleus.

The onboard Rosetta Plasma Consortium (RPC)/ Ion and Electron Sensor (IES) is capable of measuring the electron energy spectra in the energy range 1 eV/e to 22 keV/e (Burch et al. 2007). Since both CO Cameron band and [OI] 1356 Å emission lines are governed mainly by electron impact excitation reactions, the observed emission intensities may be supportive for the IES measured suprathermal electron intensity at around 15 eV.

#### 4.5. Implication of molecular oxygen in determining the G/R ratio

Molecular oxygen is the major source for the production of  $O(^1S)$  and  $O(^1D)$  in the terrestrial atmosphere. The recent discovery of  $O_2$  in 67P's coma by ROSINA/DFMS (Bieler et al. 2015) demands the inclusion of  $O_2$  in the model in order to calculate green and red-doublet emission intensities. By including 4% molecular oxygen with respect to water production rate, and for the input conditions described in Section 2, the G/R ratio is found to be increase by around 20% close to the nucleus ( $< 20$  km projected distance). Bieler et al. (2015) observed that the relative abundance of molecular oxygen ranges 1 to 10% with respect to  $H_2O$  production rate. Hence in order to determine  $CO_2$  abundance based on the G/R ratio the contribution from molecular oxygen should also be considered. In case of higher  $O_2$  abundance in comets, the observed G/R ratio can be significantly controlled by photodissociation of  $O_2$  and may lead to underestimation of  $CO_2$  mixing ratio.

#### 4.6. Parameters which can influence the predicted emission intensities

The estimated diamagnetic cavity on the sunlit side of this comet at perihelion is around 30–40 km (Benna & Mahaffy 2006; Hansen et al. 2007; Koenders et al. 2015). The extent of diamagnetic cavity depends on the gas production rate and solar wind conditions during comet perihelion visit. Beyond this cavity, most of the ions are transported towards the tail side due to solar wind interaction. The assessment of solar wind interaction on the emission intensities is beyond the scope of this work but we would like to discuss the possible sources that can alter the emission intensities. Outside the diamagnetic cavity, the chemical lifetime of neutrals can be significantly altered by charge exchange between solar wind ions and cometary species. Hence, it is expected that the calculated intensities outside the diamagnetic cavity can be changed based on the solar wind conditions during that time. The electrons outside the diamagnetic cavity are primarily solar wind electrons or shocked solar wind electrons (Reme 1991; Gringauz et al. 1986; Gan & Cravens 1990; Cravens 1991; Ip 2004). The population of suprathermal electrons outside the diamagnetic cavity is a complex problem due to admixture of solar wind electrons. However, the radius of collisional zone and diamagnetic cavity are subjected to the gas production rate and solar wind conditions during the comet perihelion passage.

For electron impact driven emissions, such as CO Cameron band and [OI] 1356 Å, due to strong solar wind interaction both neutral density and electron population may change outside the diamagnetic cavity region, thus the observed emission intensities vary significantly. In this region the solar wind electrons may also contribute to the total emission intensity (Bhardwaj et al. 1990, 1996; Bhardwaj 1999). However, the dissociative recombination CO-bearing ions to the total emission intensity contribute little (<5%), whereas formation of atomic oxygen significantly (50%), because of charge exchange between  $O^+$  and  $OH^+$  with  $H_2O$ . We do not expect the radiative decay and collisional

quenching of  $O(^1D)$  can be altered significantly due to solar wind interaction.

The evolution of cometary ionosphere around 67P nucleus has been monitored by Rosetta Plasma Consortium and Rosetta Orbiter Spectrometer for Ion and Neutral Analysis (ROSINA) instruments. The recent observations of ROSINA/Double Focussing Mass Spectrometer (DFMS), RPC/Ion and Electron Sensor (IES), and RPC/Ion Composition Analyzer (ICA), when the comet was beyond 2 AU, have shown that due to low outgassing rate no contact surface is formed and most of the solar wind has directly accessed the 67P’s nucleus, though the plasma close to the comet is dominated by cometary water ions (Fuselier et al. 2015; Broiles et al. 2015; Nilsson et al. 2015). Clark et al. (2015) found that the suprathermal electrons are accelerated to several hundreds of eV. The high energetic solar wind charged particles may also be involved in producing the excited atomic and molecular states discussed here.

The formation  $O(^1S)$ ,  $O(^1D)$ , and  $C(^1D)$  are mainly due to photochemical reactions. The contribution from ions and thermal electron recombination reactions for the inner coma is very small ( $<5\%$ ). Hence, we do not expect the predicted oxygen visible and [CI] 1931 Å line emission intensities to change due to solar wind interaction for the inner coma unless the radial distribution of  $H_2O$  is changed.

In this model we have accounted for main parent oxygen- and carbon-bearing species to compute the emission intensities. However, the contribution from photodissociation and electron impact of other minor species is also possible. In case of atomic oxygen visible emissions, the dissociation of other oxygen-bearing species, such as  $HCOOH$  or  $H_2CO$ , are unlikely to be the parent because they cannot decay fast enough to produce  $O(^1D)$  and  $O(^1S)$  (Festou & Feldman 1981). However, in the case of carbon emissions there could be an involvement from other carbon-bearing species, such as hydrocarbons. Since the major processes governing these emissions are via photochemical reactions, the role of electron



temperature for the inner coma is not significant ( $<5\%$ ). The model calculations are done for gas phase so scattering of solar photons by dust grains could be a significant factor in governing these emission intensities.

The recent ROSINA/DFMS observations on 67P show that the cometary coma contains a variety of species with heterogeneous distribution which varies with time and latitude (e.g., Hässig et al. 2015; Le Roy et al. 2015). The Microwave Instrument on the Rosetta Orbiter (MIRO) mapped around 67P’s nucleus when it was at 3.4 AU (Biver et al. 2015; Lee et al. 2015). The water column density in the inner coma (within 3 km from the nucleus) is found to vary even by two orders of magnitude. Luspay-Kuti et al. (2015) further investigated the heterogeneity of 67P’s coma by measuring various major ( $\text{H}_2\text{O}$ ,  $\text{CO}_2$ , and  $\text{CO}$ ) and minor ( $\text{HCN}$ ,  $\text{CH}_3\text{OH}$ ,  $\text{CH}_4$ , and  $\text{C}_2\text{H}_6$ ) volatile species using ROSINA/DFMS. Our calculated emission intensities may change significantly due to variable neutral densities around comet 67P. Future work will include the use of in-situ measured neutral densities from ROSINA sensors to drive model calculated emission intensities. Results could then be compared with ALICE and OSIRIS observations as well as ground-based observations.

## 5. Conclusions

Rosetta-remote and Earth-based spectroscopic observations, combined with modelling of comet 67P, offer a unique opportunity to assess the main production and destruction processes governing various forbidden visible and ultraviolet emissions as the comet gets closer to the Sun. The combined analysis applied to Rosetta remote and in-situ observations could be used as a ground truth for the interpretation of Earth-based observations on 67P cometary coma. The model calculations suggest that the electron impact reactions are the dominant sources in producing CO Cameron band emission. Hence, the observed CO Cameron emission intensity close to the cometary nucleus can be used to track the

suprathermal electron intensity in the energy range 10 to 15 eV close to the nucleus. The observed G/R ratio away from the collisional zone can be used to confirm the parent oxygen species producing these emissions. Measurement of the G/R ratio close to the comet as a function of projected distance can be used to constrain the  $\mu_w(\text{CO}_2)$ . Presence of high mixing ratio of molecular oxygen can affect the G/R ratio significantly which may lead to underestimation of  $\mu_w(\text{CO}_2)$ . The observation of [OI] 1356 Å can give a clear indication of the role of electron impact processes in the coma, while [CI] 1931 Å emission is a good tracer to probe CO distribution near the nucleus. Both Cameron band and atomic oxygen emission observations are useful to assess  $\text{H}_2\text{O}$ ,  $\text{CO}_2$ , and CO volume mixing ratios in the coma and to understand the spatial distribution and their time evolution in comet 67P. The quantitative assessment of different excitation processes is essential to study the evolution of the chemistry in the inner cometary coma with the increasing neutral gas production rate.

S.R. and M.G. acknowledge the support of the Science and Technology Facilities Council (STFC) of UK through the Consolidated Grant ST/K001051/1 to Imperial College London. The work of A.B. is supported by Indian Space Research Organization.

## REFERENCES

- Altwegg, K., Balsiger, H., Bar-Nun, A., et al. 2015, *Science*, 347, A387
- Balsiger, H., Altwegg, K., Bochsler, P., et al. 2007, *Space Sci. Rev.*, 128, 745
- Benna, M., & Mahaffy, P. R. 2006, *Geophys. Res. Lett.*, 33, 10103
- Bhardwaj, A. 1999, *J. Geophys. Res.*, 104, 1929
- . 2003, *Geophys. Res. Lett.*, 30, 2244
- Bhardwaj, A., Haider, S. A., & Singhal, R. P. 1990, *Icarus*, 85, 216
- . 1996, *Icarus*, 120, 412
- Bhardwaj, A., & Raghuram, S. 2011, *MNRAS*, 412, L25
- . 2012, *ApJ*, 748, 13
- Bieler, A., Altwegg, K., Balsiger, H., et al. 2015, *Nature*, 678
- Biver, N., Hofstadter, M., Gulkis, S., et al. 2015, *A&A*, 583, A3
- Bockelée-Morvan, D., Crovisier, J., Mumma, M. J., & Weaver, H. A. 2004, The composition of cometary volatiles: *Comets II*, ed. Festou, M. C., Keller, H. U., & Weaver, H. A., 391–423
- Broiles, T. W., Burch, J. L., Clark, G., et al. 2015, *A&A*, 583, A21
- Burch, J. L., Goldstein, R., Cravens, T. E., et al. 2007, *Space Sci. Rev.*, 128, 697
- Capria, M. T., Cremonese, G., Bhardwaj, A., & de Sanctis, M. C. 2005, *A&A*, 442, 1121
- Capria, M. T., Cremonese, G., Bhardwaj, A., Sanctis, M. C. D., & Epifani, E. M. 2008, *A&A*, 479, 257

- Capria, M. T., Cremonese, G., & de Sanctis, M. C. 2010, *A&A*, 522, A82
- Clark, G., Broiles, T. W., Burch, J. L., et al. 2015, *A&A*, 583, A24
- Cochran, A. L. 2008, *Icarus*, 198, 181
- Cochran, A. L., & Cochran, W. D. 2001, *Icarus*, 154, 381
- Cochran, W. D. 1984, *Icarus*, 58, 440
- Cravens, T. E. 1991, in *Astrophysics and Space Science Library*, Vol. 167, IAU Colloq. 116: Comets in the post-Halley era, ed. R. L. Newburn, Jr., M. Neugebauer, & J. Rahe, 1211–1255
- Cravens, T. E., & Green, A. E. S. 1978, *Icarus*, 33, 612
- Decock, A., Jehin, E., Hutsemékers, D., & Manfroid, J. 2013, *A&A*, 555, A34
- Decock, A., Jehin, E., Rousselot, P., et al. 2015, *A&A*, 573, A1
- Dello Russo, N., Mumma, M. J., Disanti, M. A., et al. 2000, *Icarus*, 143, 324
- Delsemme, A. H., & Combi, M. R. 1976, *ApJ*, 209, L149
- Delsemme, A. H., & Combi, M. R. 1979, *ApJ*, 228, 330
- Feldman, P. D. 1978, *A&A*, 70, 547
- Feldman, P. D., & Brune, W. H. 1976, *ApJ*, 209, L45
- Feldman, P. D., Cochran, A. L., & Combi, M. R. 2004, *Spectroscopic investigations of fragment species in the coma: Comets II* (M. C. Festou, H. A. Weaver, & H. U. Keller (Ed.)(Tucson: Univ. of Arizona)), 425–447

- Feldman, P. D., Festou, M. C., Tozzi, G. P., Feldman, P. D., & Weaver, H. A. 1997, *ApJ*, 475, 829
- Feldman, P. D., Weaver, H. A., Festou, M., et al. 1980, *Nature*, 286, 132
- Feldman, P. D., Steffl, A. J., Parker, J. W., et al. 2011, *Icarus*, 214, 394
- Feldman, P. D., M. F. A’Hearn, J.-L. Bertaux, et al. 2015, *A&A*, doi:10.1051/0004-6361/201525925
- Festou, M. C., & Feldman, P. D. 1981, *A&A*, 103, 154
- Fink, U., & Johnson, J. R. 1984, *AJ*, 89, 1565
- Furusho, R., Kawakita, H., Fuse, T., & Watanabe, J. 2006, *Adv. Space Res.*, 9, 1983
- Fuselier, S. A., Altwegg, K., Balsiger, H., et al. 2015, *A&A*, 583, A2
- Gan, L., & Cravens, T. E. 1990, *J. Geophys. Res.*, 95, 6285
- Gilijamse, J. J., Hoekstra, S., Meek, S. A., et al. 2007, *J. Chem. Phys.*, 127, 221102
- Gringauz, K. I., Gombosi, T. I., Remizov, A. P., et al. 1986, *Nature*, 321, 282
- Gulkis, S., Allen, M., von Allmen, P., et al. 2015, *Science*, 347, 709
- Hansen, K., Bagdonat, T., Motschmann, U., et al. 2007, *Space Sci. Rev.*, 128, 133
- Haser, L. 1957, *Bulletin de la Societe Royale des Sciences de Liege*, 43, 740
- Hässig, M., Altwegg, K., Balsiger, H., et al. 2015, *Science*, 347, aaa0276
- Hibbert, A., Biemont, E., Godefroid, M., & Vaeck, N. 1993, *A&AS*, 99, 179
- Huestis, D. L., & Slanger, T. G. 2006, in *Bulletin of the American Astronomical Society*, Vol. 38, AAS/Division for Planetary Sciences Meeting Abstracts #38, 609

- Ip, W.-H. 2004, Global solar wind interaction and ionospheric dynamics, ed. Festou, M. C., Keller, H. U., & Weaver, H. A., 605–629
- Johnson, C. E. 1972, *Phys. Rev. A*, 5, 2688
- Keller, H. U., Barbieri, C., Lamy, P., et al. 2007, *Space Sci. Rev.*, 128, 433
- Koenders, C., Glassmeier, K.-H., Richter, I., Ranocha, H., & Motschmann, U. 2015, *Planet. Space. Sci.*, 105, 101
- Körösmezey, A., Cravens, T. E., Gombosi, T. I., et al. 1987, *J. Geophys. Res.*, 92, 7331
- Le Roy, L., Altwegg, K., Balsiger, H., et al. 2015, *A&A*, doi:10.1051/0004-6361/201526450
- Lee, S., von Allmen, P., Allen, M., et al. 2015, *A&A*, 583, A5
- Luspay-Kuti, A., Hässig, M., Fuselier, S. A., et al. 2015, *A&A*, 583, A4
- Makarov, O. P., Ajello, J. M., Vattipalle, P., et al. 2004, *Journal of Geophysical Research (Space Physics)*, 109, 9303
- McKay, A. J., Chanover, N. J., Morgenthaler, J. P., et al. 2012, *Icarus*, 277
- McKay, A. J., Chanover, N. J., Morgenthaler, J. P., et al. 2013, *Icarus*, 222, 684
- McKay, A. J., Cochran, A. L., DiSanti, M. A., et al. 2015, *Icarus*, 250, 504
- McPhate, J. B., Feldman, P. D., McCandliss, S. R., & Burgh, E. B. 1999, *ApJ*, 521, 920
- Morgenthaler, J. P., Harris, W. M., Scherb, F., et al. 2001, *ApJ*, 563, 451
- Morrison, N. D., Knauth, D. C., Mulliss, C. L., & Lee, W. 1997, *Astro. Soc. Pac.*, 109, 676
- Mumma, M. J., & Charnley, S. B. 2011, *ARAA*, 49, 471
- Mumma, M. J., DiSanti, M. A., Dello Russo, N., et al. 1996, *Science*, 272, 1310

- Mumma, M. J., Disanti, M. A., Tokunaga, A. T., & Roettger, E. E. 1995, in Bulletin of the American Astronomical Society, Vol. 27, AAS/Division for Planetary Sciences Meeting Abstracts #27, 1144
- Nilsson, H., Stenberg Wieser, G., Behar, E., et al. 2015, A&A, 583, A20
- Oliversen, R. J., Doane, N., Scherb, F., Harris, W. M., & Morgenthaler, J. P. 2002, ApJ, 581, 770
- Raghuram, S., & Bhardwaj, A. 2012, Planet. Space Sci., 63, 139
- . 2013, Icarus, 223, 91
- . 2014, A&A, 566, A134
- Reme, H. 1991, Washington DC American Geophysical Union Geophysical Monograph Series, 61, 87
- Rubin, M., Altwegg, K., Balsiger, H., et al. 2015, Science, 348, 232
- Sahnou, D. J., Feldman, P. D., McCandliss, S. R., & Martinez, M. E. 1993, Icarus, 101, 71
- Schultz, D., Li, G. S. H., Scherb, F., & Roesler, F. L. 1992, Icarus, 96, 190
- Sierks, H., Barbieri, C., Lamy, P. L., et al. 2015, Science, 347, 1044
- Smith, A. M., Stecher, T. P., & Casswell, L. 1980, ApJ, 242, 402
- Snodgrass, C., Tubiana, C., Bramich, D. M., et al. 2013, A&A, 557, A33
- Stern, S. A., Slater, D. C., Scherrer, J., et al. 2007, Space Sci. Rev., 128, 507
- Tozzi, G. P., Feldman, P. D., & Festou, M. C. 1998, A&A, 330, 753
- Vigren, E., & Galand, M. 2013, ApJ, 772, 33

- Weaver, H. A., Feldman, P. D., McPhate, J. B., et al. 1994, *ApJ*, 422, 374
- Weaver, H. A., Feldman, P. D., A’Hearn, M. F., et al. 1997, *Science*, 275, 1900
- Whipple, F. L., & Huebner, W. F. 1976, *ARA&A*, 14, 143
- Woods, T. N., Feldman, P. D., Dymond, K. F., & Sahnow, D. J. 1986, *Nature*, 324, 436
- Woods, T. N., Eparvier, F. G., Bailey, S. M., et al. 2005, *Journal of Geophysical Research* (Space Physics), 110, 1312
- Zhang, H. W., Zhao, G., & Hu, J. Y. 2001, *A&A*, 367, 1049



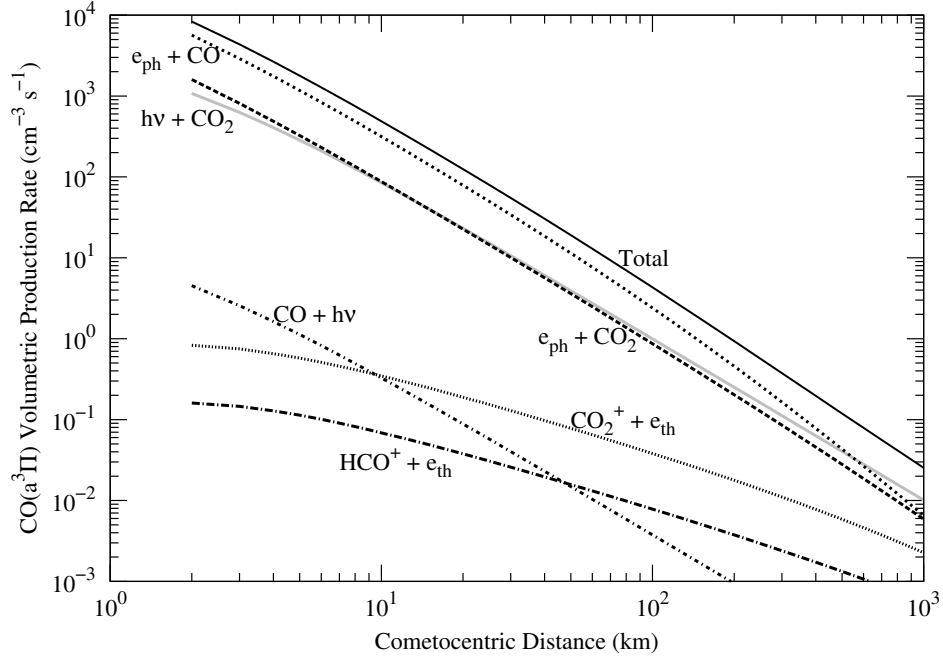


Fig. 1.— The calculated  $\text{CO}(\text{a}^3\Pi)$  rate profiles in comet 67P/Churyumov-Gerasimenko for an  $\text{H}_2\text{O}$  out gassing rate of  $10^{28} \text{ s}^{-1}$  and for 5%  $\text{CO}_2$  and 5%  $\text{CO}$  volumetric mixing ratios relative to water at 1.29 AU. The photodissociation of  $\text{CO}_2$  (gray curve) and suprathermal electron impact on  $\text{CO}_2$  (solid dashed curve) are producing  $\text{CO}(\text{a}^3\Pi)$  with nearly equal rates and both curves overlap.  $h\nu$ ,  $e_{th}$ , and  $e_{ph}$  stand for photon, thermal electron, and suprathermal electron, respectively.

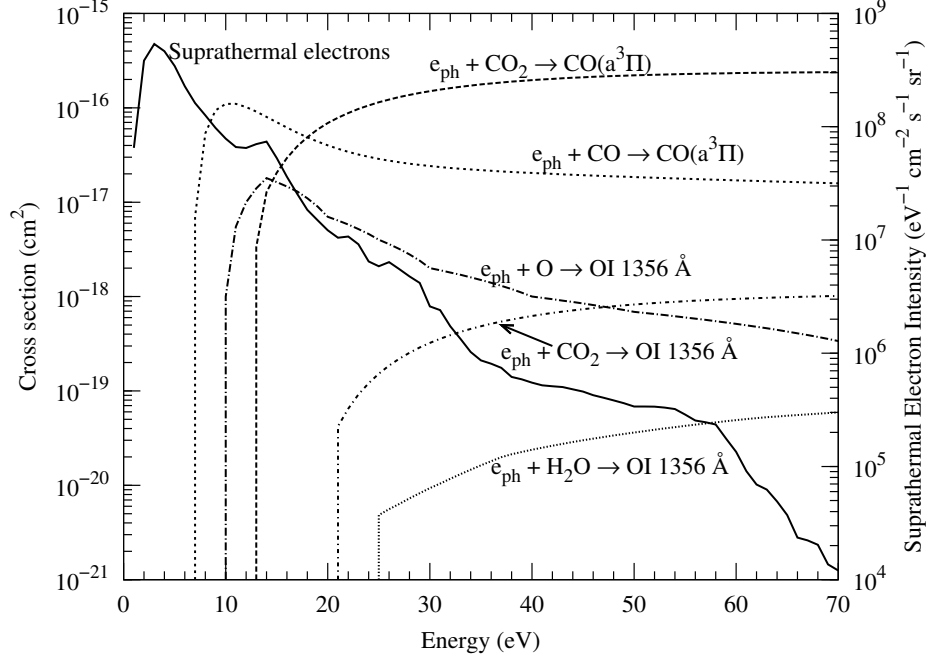


Fig. 2.— Cross sections for electron impact excitation of  $\text{CO}(\text{a}^3\Pi)$  from  $\text{CO}$  and  $\text{CO}_2$ , and for  $[\text{OI}]$  1356 Å from atomic oxygen,  $\text{CO}_2$ , and  $\text{H}_2\text{O}$ . Calculated suprathermal electron intensity at cometocentric distance of 10 km is also shown with magnitude on right side y-axis. The cross section for the formation of  $[\text{OI}]$  1356 Å emission line from electron impact dissociation of  $\text{H}_2\text{O}$  is estimated by taking the ratio of cross sections for  $\text{OI}$  1304 Å to  $[\text{OI}]$  1356 Å at 100 eV from Makarov et al. (2004).  $e_{ph}$  stand for suprathermal electron.

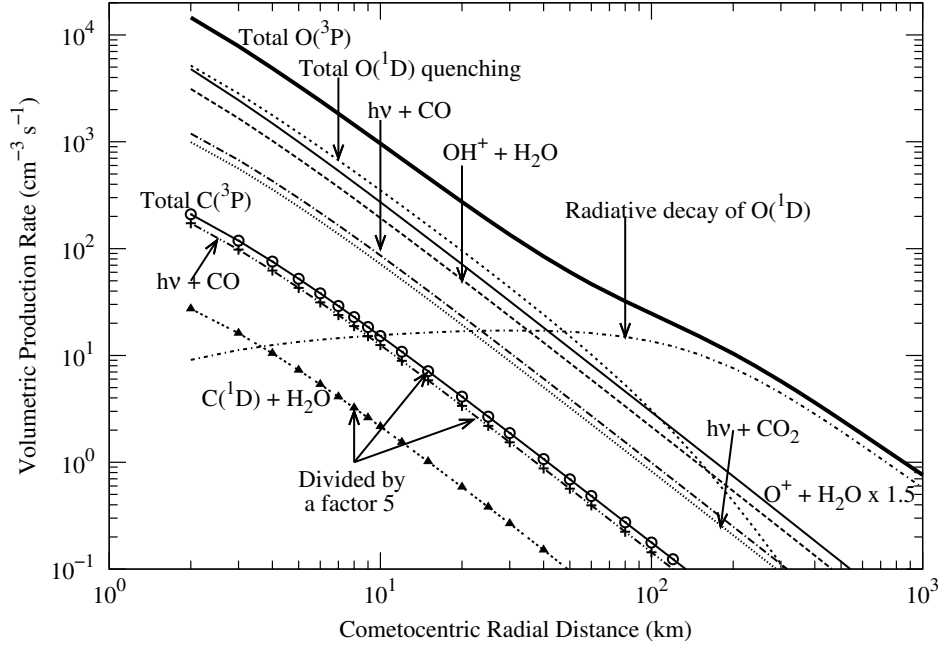


Fig. 3.— The calculated atomic oxygen and atomic carbon production rate profiles in comet 67P/Churyumov-Gerasimenko with the water production rate of  $10^{28} \text{ s}^{-1}$  for 5%  $\text{CO}_2$  and 5% CO volume mixing ratios relative to water at 1.29 AU. The calculated atomic carbon production rate profiles, which are represented with symbols and curves, are divided by a factor 5. The production rate profile of  $\text{O}(^3\text{P})$  through charge exchange between  $\text{O}^+$  and  $\text{H}_2\text{O}$  is multiplied by a factor 1.5.  $h\nu$  stand for photon.

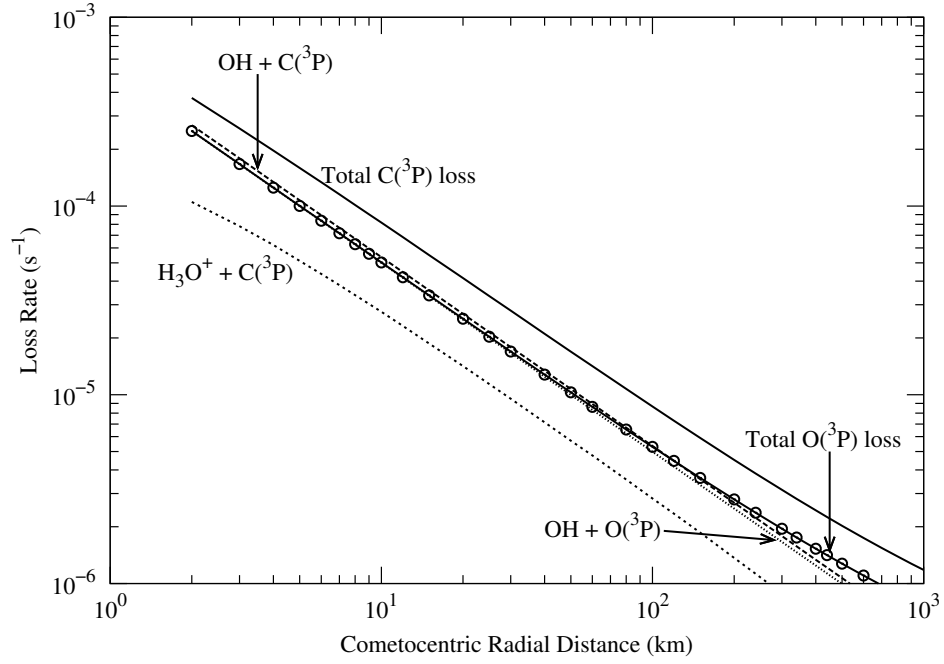


Fig. 4.— The calculated atomic oxygen and atomic carbon loss rate profiles in comet 67P/Churyumov-Gerasimenko with the water production rate of  $10^{28} \text{ s}^{-1}$  for 5%  $\text{CO}_2$  and 5%  $\text{CO}$  volume mixing ratios relative to water at 1.29 AU.

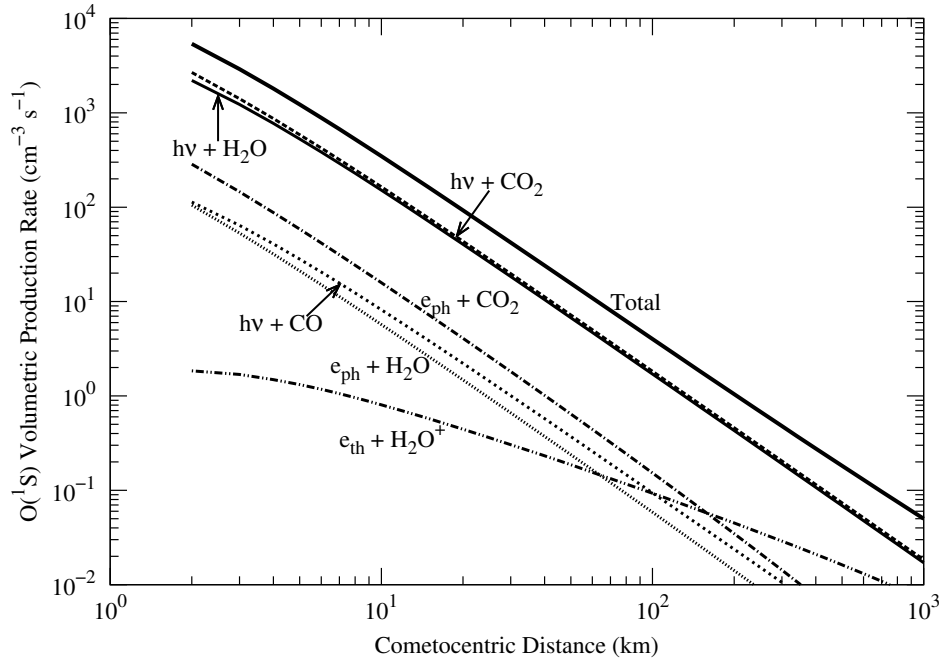


Fig. 5.— The calculated  $O(^1S)$  rate profiles in comet 67P/Churyumov-Gerasimenko for an  $H_2O$  out gassing rate of  $10^{28} \text{ s}^{-1}$  and for 5%  $CO_2$  and 5%  $CO$  volumetric mixing ratios relative to water at 1.29 AU.  $h\nu$ ,  $e_{ph}$ , and  $e_{th}$  stand for photon, thermal electron, and suprathermal electron, respectively.

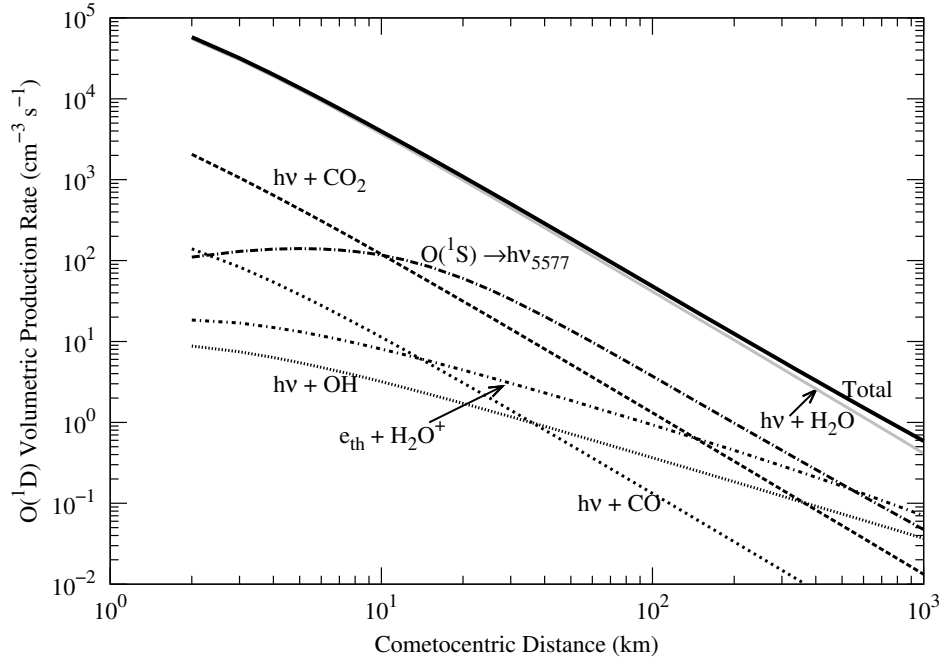


Fig. 6.— The calculated  $O(^1D)$  rate profiles in comet 67P/Churyumov-Gerasimenko with the water production rate of  $10^{28} \text{ s}^{-1}$  for 5%  $\text{CO}_2$  and 5%  $\text{CO}$  volume mixing ratios relative to water at 1.29 AU.  $h\nu$  and  $e_{ph}$  stand for photon and thermal electron, respectively.

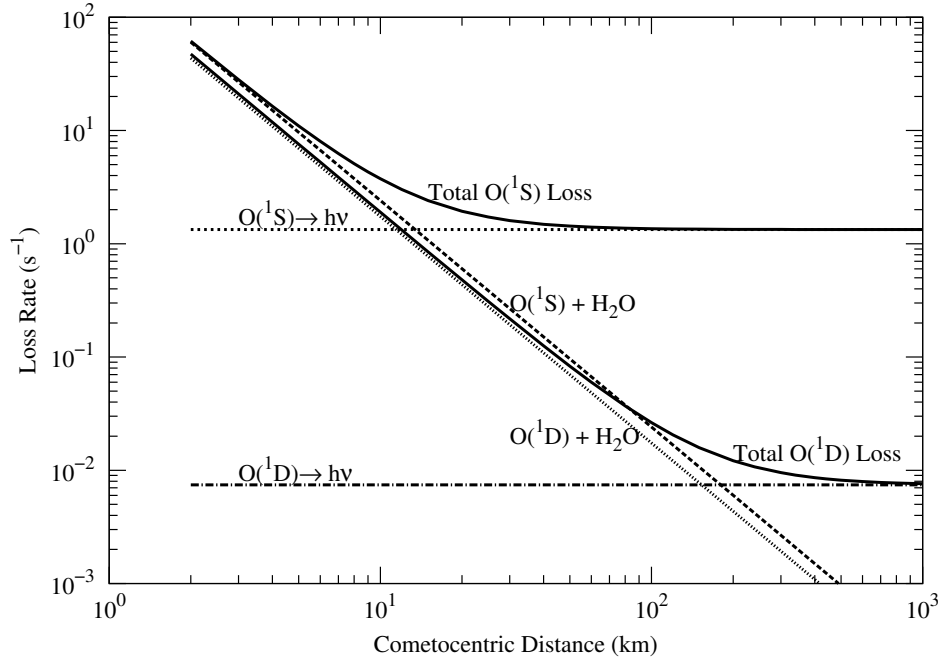


Fig. 7.— The calculated  $\text{O}(^1\text{S})$  and  $\text{O}(^1\text{D})$  loss rate profiles in comet 67P/Churyumov-Gerasimenko with the water production rate of  $10^{28} \text{ s}^{-1}$  for 5%  $\text{CO}_2$  and 5%  $\text{CO}$  volume mixing ratios relative to water at 1.29 AU.  $h\nu$  stand for photon.

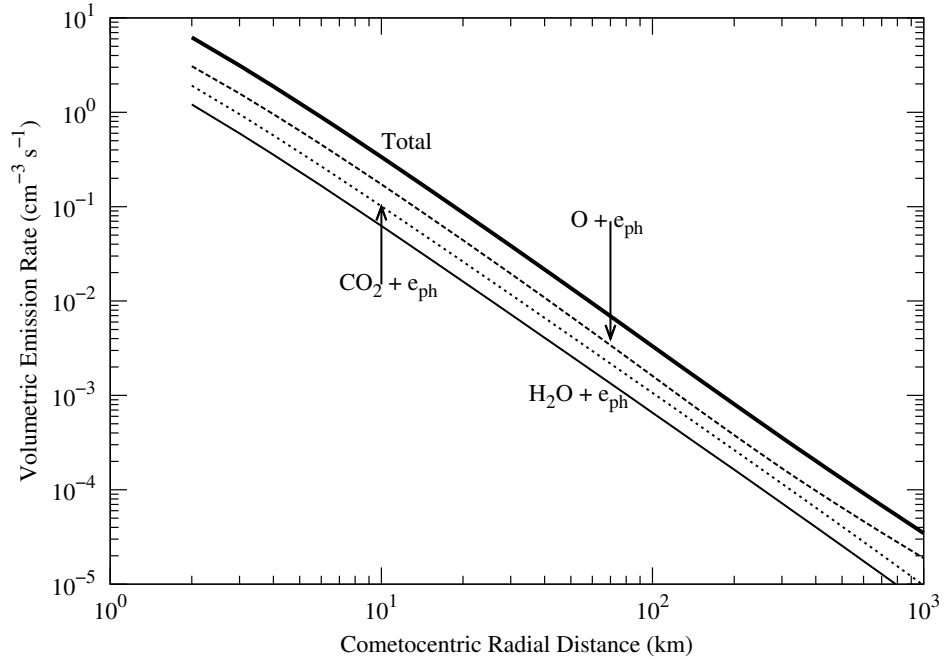


Fig. 8.— The calculated [OI] 1356 Å emission rate profiles in comet 67P/Churyumov-Gerasimenko with the water production rate of  $10^{28} \text{ s}^{-1}$  for 5% CO<sub>2</sub> and 5% CO volume mixing ratios relative to water at 1.29 AU.  $e_{ph}$  stand for suprathermal electron.



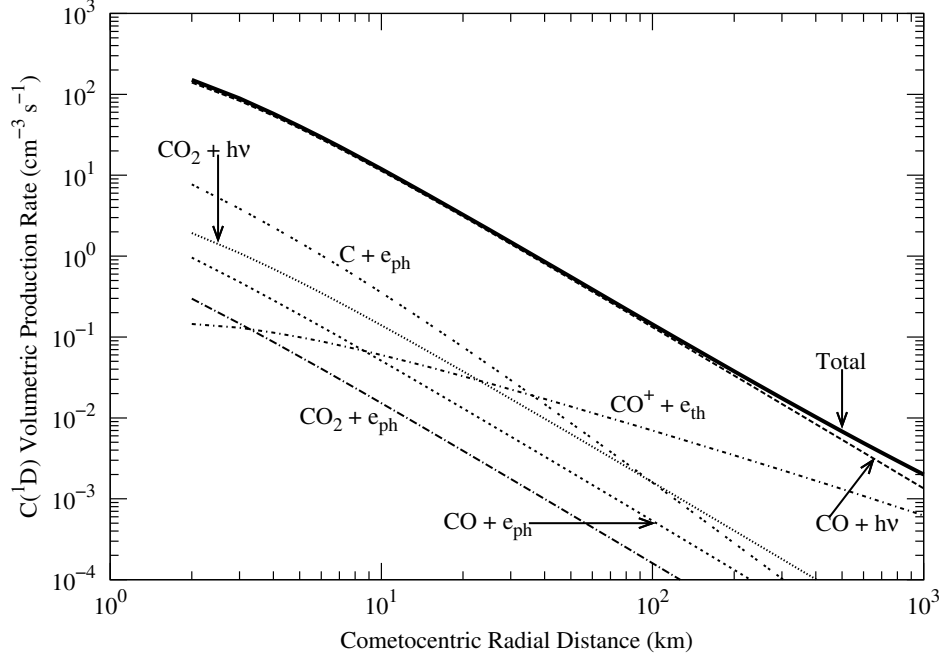


Fig. 9.— The calculated  $C(^1D)$  production rate profiles in comet 67P/Churyumov-Gerasimenko with the water outgassing rate of  $10^{28} \text{ s}^{-1}$  for 5%  $\text{CO}_2$  and 5%  $\text{CO}$  volume mixing ratios relative to water at 1.29 AU.  $h\nu$ ,  $e_{ph}$ , and  $e_{ph}$  stand for photon, thermal electron, and suprathermal electron, respectively.

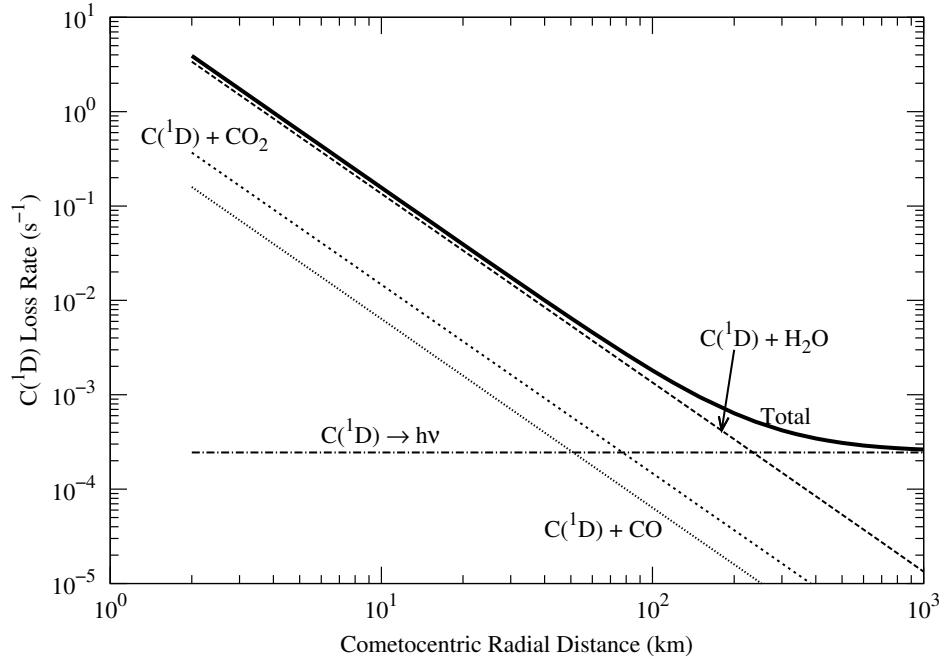


Fig. 10.— The calculated  $C(^1D)$  loss rate profiles in comet 67P/Churyumov-Gerasimenko with the water production rate of  $10^{28} \text{ s}^{-1}$  for 5%  $\text{CO}_2$  and 5%  $\text{CO}$  volume mixing ratios relative to water at 1.29 AU.  $h\nu$  stand for photon;

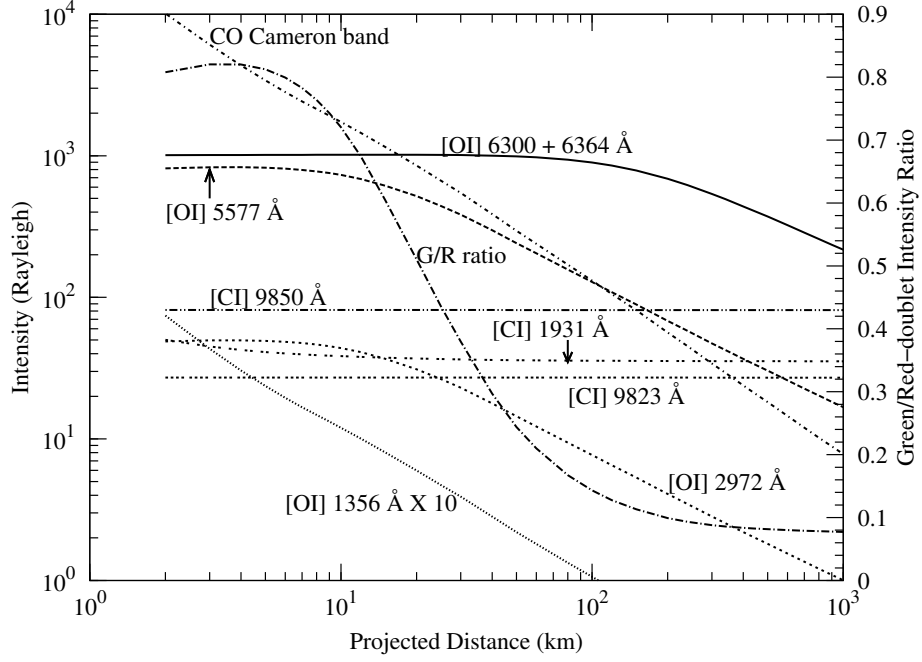


Fig. 11.— The calculated various emission intensities for 5% CO<sub>2</sub> and 5% CO volume mixing ratios relative to water in comet 67P/Churyumov-Gerasimenko with water production rate  $1 \times 10^{28} \text{ s}^{-1}$  as a function of projected distance at 1.29 AU. The calculated G/R ratio values are shown on the right Y-axis. The [OI] 1356 Å emission line profile is multiplied by a factor 10. One Rayleigh =  $\frac{10^6}{4\pi} \text{ photons cm}^{-2} \text{ s}^{-1} \text{ sr}^{-1}$ .

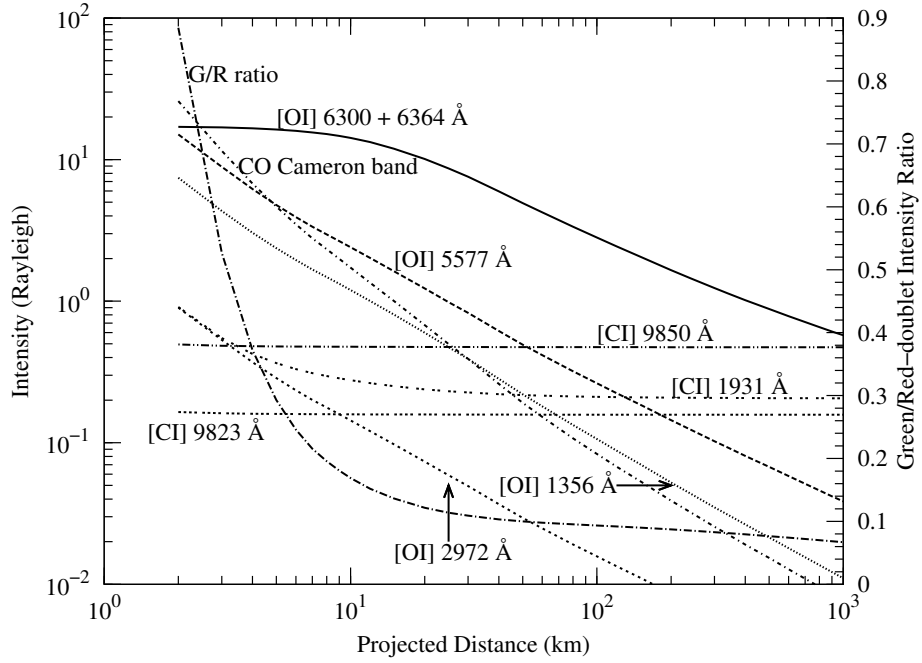


Fig. 12.— The calculated various emission intensities for 5%  $\text{CO}_2$  and 15% CO volume mixing ratios relative to water in comet 67P/Churyumov-Gerasimenko with water production rate  $5 \times 10^{25} \text{ s}^{-1}$  as a function of projected distance at 3 AU. The calculated G/R ratio values are shown on the right Y-axis. One Rayleigh =  $\frac{10^6}{4\pi} \text{ photons cm}^{-2} \text{ s}^{-1} \text{ sr}^{-1}$ .

Table 1: The calculated contribution of different production processes producing CO(a<sup>3</sup>Π) in comet 67P for different CO<sub>2</sub> and CO volume mixing ratios relative to water.

Volume mixing ratios		Percentage contribution at different projected distances (km)											
relative to water (%)		hν + CO <sub>2</sub>			e <sub>ph</sub> + CO <sub>2</sub>			e <sub>ph</sub> + CO			Others <sup>†</sup>		
CO <sub>2</sub>	CO	10	10 <sup>2</sup>	10 <sup>3</sup>	10	10 <sup>2</sup>	10 <sup>3</sup>	10	10 <sup>2</sup>	10 <sup>3</sup>	10	10 <sup>2</sup>	10 <sup>3</sup>
1	1	14.2	14.5	13.9	15.8	15.4	14.7	69.7	68.5	65.4	0.2	1.6	6.0
1	2	9.1	9.3	9.1	9.6	9.5	9.1	81.1	80.1	77.5	0.2	1.1	4.3
1	5	5.0	5.2	5.1	4.8	4.7	4.6	90.1	89.3	87.2	0.1	0.8	3.1
2	1	21.6	21.9	20.6	24.4	23.6	22.1	53.6	52.2	48.8	0.4	2.3	8.5
2	2	15.2	15.5	14.8	16.3	15.9	15.1	68.3	66.9	63.7	0.3	1.7	6.4
2	5	9.0	9.3	9.1	8.7	8.6	8.3	82.1	81.0	78.2	0.2	1.1	4.5
5	1	31.4	31.5	28.9	36.5	34.8	31.7	31.6	30.4	27.7	0.5	3.3	11.7
5	2	25.2	25.5	23.8	28.0	26.9	24.9	46.4	44.9	41.6	0.4	2.7	9.8
5	5	17.3	17.7	16.9	17.4	16.9	15.9	65.0	63.4	59.9	0.3	2.0	7.3
0	1	0.0	0.0	0.0	0.0	0.0	0.0	100.0	99.8	99.0	0.0	0.2	1.0
0	2	0.0	0.0	0.0	0.0	0.0	0.0	100.0	99.8	98.9	0.0	0.2	1.0
0	5	0.0	0.0	0.0	0.0	0.0	0.0	100.0	99.7	98.7	0.0	0.3	1.3
1	0	45.3	44.6	39.5	54.0	50.9	45.0	0.0	0.0	0.0	0.7	4.5	15.5
2	0	45.1	44.5	39.4	54.2	51.1	45.1	0.0	0.0	0.0	0.8	4.5	15.5
5	0	44.5	44.0	39.0	54.7	51.5	45.4	0.0	0.0	0.0	0.8	4.5	15.6

<sup>†</sup>Others corresponds to sum of contributions from dissociative recombination of HCO<sup>+</sup> and CO<sub>2</sub><sup>+</sup> ions and resonance fluorescence of CO.

Table 2: The calculated contribution of different production processes producing O(<sup>1</sup>S) and O(<sup>1</sup>D) in comet 67P for different CO<sub>2</sub> and CO volume mixing ratios relative to water.

Volume mixing ratios		Percentage contribution at different projected distances (km)										G/R ratio	
relative to water (%)		hν + H <sub>2</sub> O		hν + CO <sub>2</sub> [ hν + OH]		Others <sup>†</sup>							
CO <sub>2</sub>	CO	10	10 <sup>2</sup>	10 <sup>3</sup>	10	10 <sup>2</sup>	10 <sup>3</sup>	10	10 <sup>2</sup>	10 <sup>3</sup>	10	10 <sup>2</sup>	10 <sup>3</sup>
1	1	75.1[94.6] <sup>†</sup>	67.3[83.9]	44.3[54.2]	16.4[0.8]	14.5[5.4]	9.8[24.5]	8.5[4.6]	18.2[10.6]	45.9[21.3]	0.41	0.09	0.05
1	2	74.3[94.5]	66.6[83.9]	43.8[54.2]	16.2[0.8]	14.3[5.4]	9.6[24.5]	9.5[4.7]	19.1[10.7]	46.6[21.3]	0.42	0.09	0.05
1	5	71.7[94.3]	64.2[83.6]	42.1[54.0]	15.6[0.8]	13.8[5.4]	9.3[24.5]	12.6[4.9]	22.0[10.9]	48.7[21.5]	0.44	0.09	0.05
2	1	63.3[93.5]	57.2[82.7]	38.7[53.5]	27.6[0.8]	24.6[5.4]	17.0[24.2]	9.1[5.8]	18.2[12.0]	44.2[22.3]	0.49	0.10	0.05
2	2	62.8[93.4]	56.8[82.6]	38.3[53.5]	27.4[0.8]	24.4[5.4]	16.9[24.2]	9.8[5.8]	18.9[12.0]	44.8[22.3]	0.49	0.10	0.05
2	5	61.2[93.2]	55.2[82.4]	37.1[53.3]	26.6[0.8]	23.7[5.3]	16.3[24.1]	12.2[6.1]	21.1[12.3]	46.6[22.5]	0.51	0.10	0.06
5	1	43.2[90.2]	39.5[79.0]	28.0[51.4]	46.7[0.8]	42.3[5.1]	30.8[23.3]	10.2[9.1]	18.2[15.8]	41.2[25.3]	0.69	0.14	0.07 <sup>46</sup>
5	2	43.0[90.1]	39.3[79.0]	27.9[51.4]	46.5[0.8]	42.2[5.1]	30.7[23.3]	10.4[9.1]	18.5[15.9]	41.5[25.3]	0.69	0.14	0.07
5	5	42.5[89.9]	38.7[78.8]	27.3[51.3]	45.8[0.8]	41.6[5.1]	30.1[23.2]	11.7[9.3]	19.7[16.0]	42.6[25.5]	0.71	0.14	0.07
0	1	92.4[95.8]	81.7[85.3]	51.8[54.9]	0.0[0.8]	0.0[5.5]	0.0[24.9]	7.6[3.4]	18.3[9.2]	48.2[20.2]	0.34	0.07	0.04
0	2	90.9[95.7]	80.4[85.2]	51.0[54.9]	0.0[0.8]	0.0[5.5]	0.0[24.9]	9.1[3.5]	19.6[9.3]	49.0[20.2]	0.35	0.07	0.04
0	5	86.8[95.4]	76.8[84.9]	48.6[54.8]	0.0[0.8]	0.0[5.5]	0.0[24.8]	13.2[3.8]	23.2[9.6]	51.4[20.4]	0.36	0.08	0.04
1	0	75.9[94.7]	68.0[84.0]	44.8[54.2]	16.6[0.8]	14.6[5.4]	9.9[24.5]	7.5[4.5]	17.4[10.6]	45.3[21.3]	0.41	0.08	0.05
2	0	63.8[93.5]	57.6[82.7]	39.0[53.5]	27.8[0.8]	24.8[5.4]	17.2[24.2]	8.4[5.7]	17.6[11.9]	43.8[22.4]	0.48	0.10	0.05
5	0	43.2[90.2]	39.5[79.1]	28.1[51.4]	46.7[0.8]	42.4[5.1]	30.9[23.3]	10.1[9.0]	18.1[15.8]	41.0[25.4]	0.69	0.14	0.07

<sup>†</sup>The values in the square brackets are for O(<sup>1</sup>D); <sup>‡</sup>Others corresponds to the sum of the contributions from all reactions listed in Tables 1 and 2 of Bhardwaj & Raghuram (2012) for the formation of O(<sup>1</sup>S) and O(<sup>1</sup>D) except photodissociation of H<sub>2</sub>O and CO<sub>2</sub>.